THE JOURNAL OF PHYSICAL CHEMISTRY B

ARTICLE

pubs.acs.org/JPCB

Ensemble and Single-Molecule Spectroscopic Study on Excitation Energy Transfer Processes in 1,3-Phenylene-Linked Perylenebisimide Oligomers

Hee Won Bahng,[†] Min-Chul Yoon,[†] Ji-Eun Lee,[†] Yuichi Murase,[‡] Tomoki Yoneda,[‡] Hiroshi Shinokubo,[§] Atsuhiro Osuka,[*,‡] and Dongho Kim[*,†]

[†]Spectroscopy Laboratory for Functional π-Electronic Systems and Department of Chemistry, Yonsei University, Seoul 120-749, Korea

[‡]Department of Chemistry and Graduate School of Science, Kyoto University, Sakyo-ku, Kyoto 606-8502, Japan

[§]Department of Applied Chemistry, Graduate School of Engineering, Nagoya University, Chikusa-ku, Nagoya 464-8603, Japan

Supporting Information

ABSTRACT: 1,3-Phenylene-bridged perylenebisimide dimer (**PBI2**) and trimer (**PBI3**) were prepared along with monomer reference (**PBI1**) using perylene imide-anhydride **5** as a key precursor. 3,3-Dimethylbut-1-yl substituents were introduced at the 2,5-positions of perylenebisimide (PBI) to improve the solubilities of **PBI** oligomers. Actually, no serious aggregation of **PBI2** and **PBI3** was detected in their dilute CH_2Cl_2 solutions. Under these conditions, intramolecular electronic interactions among PBI chromophores have been revealed by measuring the photophysical properties at their ensemble and single-molecule levels. The excitation energy transfer times of **PBI2** (0.16 ps) and **PBI3** (0.60 ps) were determined from the two different observables, anisotropy depolarization, and singlet−singlet annihilation, respectively, which are considered as the incoherent Förster-type energy hopping (EEH) times as compared with the EEH time constant (1.97 ps) calculated on the basis of the Förster mechanism. The relatively short EEH times compared to similar PBI oligomers can be attributed to 1,3-phenylene linker, which assures a short distance between the chromophores and, as a consequence, makes it hard to treat the PBI unit as a point dipole. The limitation of point-dipole approximation to describe the PBI oligomers and additional through-bond type interactions can be attributed as the causes of the discrepancies in excitation energy transfer times. Considering these photophysical properties, we can suggest that 1,3-phenylene-linked PBI oligomers have potentials as molecular photonic devices including the artificial light-harvesting system.

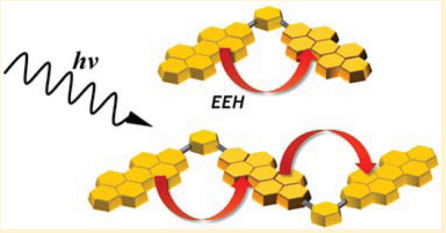

INTRODUCTION

Photosynthesis illustrating subsequent directional transport of excitation energy through energy transfer to the photosynthetic reaction center is one of the most efficient biological processes in nature.[1] This high efficiency is an outcome of the proper organization of a multitude of chromophores in space that have abilities to collect light and deliver the excitation energy. Inspired by the natural light-harvesting system, there have been numerous trials in the synthesis of artificial molecular assemblies possessing energy and charge transport properties for mimicking the fundamental processes in photosynthesis.[2,3] One of the key features in this approach is a fine control of molecular structures in terms of the excited-state properties and their organization. There have been various synthetic strategies to reproduce the light-harvesting architectures like covalently constructed and self-assembled ones.[4−6] While self-assembly is advantageous for an expansion into larger oligomers, the overall structures lack a structural rigidity. In contrast, the structural control performed by a covalent approach has advantages of robust stability and tuning ability of spatial arrangement by using connecting linkers. In this case, a cautious choice of linker will allow the precise control of molecular structures, and consequently electronic interactions between constituent chromophores.[7]

Numerous classes of functional dyes have been employed as chromophores in the mimicry of natural light-harvesting architectures. To operate as efficient excitation energy transfer architectures, these dyes should display appropriate properties.[8,9] In this respect, perylenebisimide (PBI) can be an excellent candidate because it can ensure efficient sequential energy transfer between the individual dye units possessing exceptional chemical, thermal, photochemical, and photophysical stabilities in combination with high exctinction coefficients and fluorescence quantum yields.[10,11] Indebted to these properties, a variety of multichromophric architectures composed of PBI derivatives have been envisaged and prepared for understanding of light-harvesting energy transfer processes[7,12] for practical applications in the development of new photonic devices like organic OLEDs[13] and single photon sources.[14] For the covalently linked

Received: September 14, 2011
Revised: December 22, 2011
Published: December 23, 2011

Chart 1. Molecular Structures of PBI Monomer (PBI1), Dimer (PBI2), and Trimer (PBI3)

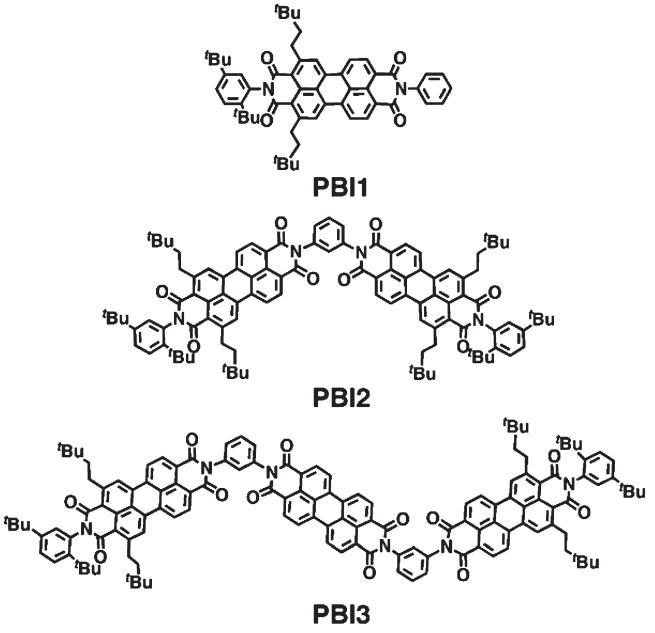

open chain architectures, various types of PBI oligomers have been produced.[7] According to the previous findings, the molecular excited states of J-type PBI linear oligomers become different depending on the distance between adjacent PBI units. When the interchromophoric distance in the PBI oligomers is close enough to induce strong dipole couplings, the coherent delocalization in the excited state is generated.[15,16] As the interchromophoric distance increases, the coupling strength becomes weak to lose the excitonic coherence, so the excitation energy transfer takes place in an incoherent way.[9] From these results, we can understand the effect of the interchromophoric distance on the excitation energy transfer dynamics in the PBI oligomers. However, H-type cofacial π-stacked PBI oligomers exhibit significant orbital overlaps between adjacent chromophores, which lead to a significant perturbation in the molecular photophysical properties.[17] Thus, it is difficult to investigate the excitation energy transfer dynamics in the PBI oligomers without a loss of the original molecular properties.

In this work, we have prepared covalently linked PBI dimer (**PBI2**) and PBI trimer (**PBI3**) along with their monomer reference (**PBI1**), whose structures are shown in Chart 1. Alkyl chains are introduced at 2,5-positions to improve the solubilities of **PBI2** and **PBI3** in common organic solvents. 1,3-Phenylene linker positions the transition dipole moments of neighboring PBI chromophores tilted at around 120°, which leads to situations that the polarization change between the ground and excited states can be examined by polarization anisotropy measurements, and the neighboring PBI units are separated in a well-defined manner to avoid serious interchromophoric interactions like excimer formation. Thus, we can observe the excited state dynamics without a drastic change in the molecular photophysical properties. Here, we have investigated the EEH processes occurring in **PBI2** and **PBI3** by time-resolved femtosecond spectroscopic techniques, using **PBI1** monomer as a reference. Femtosecond transient absorption anisotropy (TAA) measurements give direct evidence about the EEH because the initial localization of excitations in weakly coupled multichromophores gives rise to fast depolarization as the excitation energy is transferred. The observed singlet−singlet annihilation is also well associated with the EEH because this process is conceived as an incoherent energy hopping from the excited donor to the proximal excited acceptor.[5,18] Using both the anisotropy depolarization and singlet−singlet annihilation times, we were able to quantify the EEH time in PBI multichromophores. In addition, the single molecule spectroscopic technique was utilized to investigate the molecular distributions of the excitation energy transfer dynamics of PBI oligomers for a comparative analysis with the ensemble measurements.

EXPERIMENTAL SECTION

Synthesis. **PBI1**, **PBI2**, and **PBI3** were prepared according to the synthetic route shown in Scheme 1. Detailed experimental procedures are given in the Supporting Information.

Steady-State Spectroscopy. The sample solutions were prepared in approximately micromolar concentrations in dichloromethane (CH_2Cl_2). Dichloromethane was purchased from Sigma-Aldrich (spectrophotometric grade). Absorption spectra were obtained by using a UV−vis spectrometer (Cary5000, Varian), and fluorescence spectra were obtained by using a fluorometer (F-2500, Hitachi). The fluorescence quantum yields were obtained using rhodamine 6G in methanol as reference ($\Phi_f = 0.95$), with $\lambda_{ex} = 480$ nm.

Time-Resolved Fluorescence Decay and Anisotropy. A time-correlated single-photon-counting (TCSPC) system was used for measurements of spontaneous fluorescence decay and fluorescence anisotropy decay. As an excitation light source, we used a mode-locked Ti:sapphire laser (MaiTai BB, Spectra Physics), which provides an ultrashort pulse (80 fs at full width half-maximum, fwhm) with a high repetition rate (80 MHz). This high repetition rate slows down to 1 M ≈ 800 kHz by using a homemade pulse-picker. The pulse-picked output pulse was frequency-doubled by a 1 mm thickness of a BBO crystal (EKSMA). The fluorescence was collected by a microchannel plate photomultiplier (MCP-PMT, R3809U-51, Hamamatsu) with a thermoelectric cooler (C4878, Hamamatsu) connected to a TCSPC board (SPC-130, Becker & Hickel GmbH). The overall instrumental response function was about 25 ps (fwhm). A vertically polarized pump pulse by a Glan-laser polarizer was irradiated to samples, and a sheet polarizer, set at an angle complementary to the magic angle (54.7°), was placed in the fluorescence collection path to obtain polarization-independent fluorescence decays. Time-resolved fluorescence anisotropy decays were obtained by changing the detection polarization on the fluorescence path to parallel or perpendicular to the polarization of the excitation pulses. The calculation of anisotropy decay was then followed by

$$r(t) = \frac{I_{VV}(t) - GI_{VH}(t)}{I_{VV}(t) + 2GI_{VH}(t)}$$

where $I_{VV}(t)$ [or $I_{VH}(t)$] is the fluorescence decay when the excitation light is vertically polarized and only the vertically (or horizontally) polarized portion of fluorescence is detected, and the first and second subscripts represent excitation and detection polarization, respectively. The factor G is defined by $I_{HV}(t)/I_{HH}(t)$, which is equal to the ratio of the sensitivities of the detection system for vertical and horizontal polarization.

Scheme 1. Synthetic Procedure of PBI1, PBI2, and PBI3

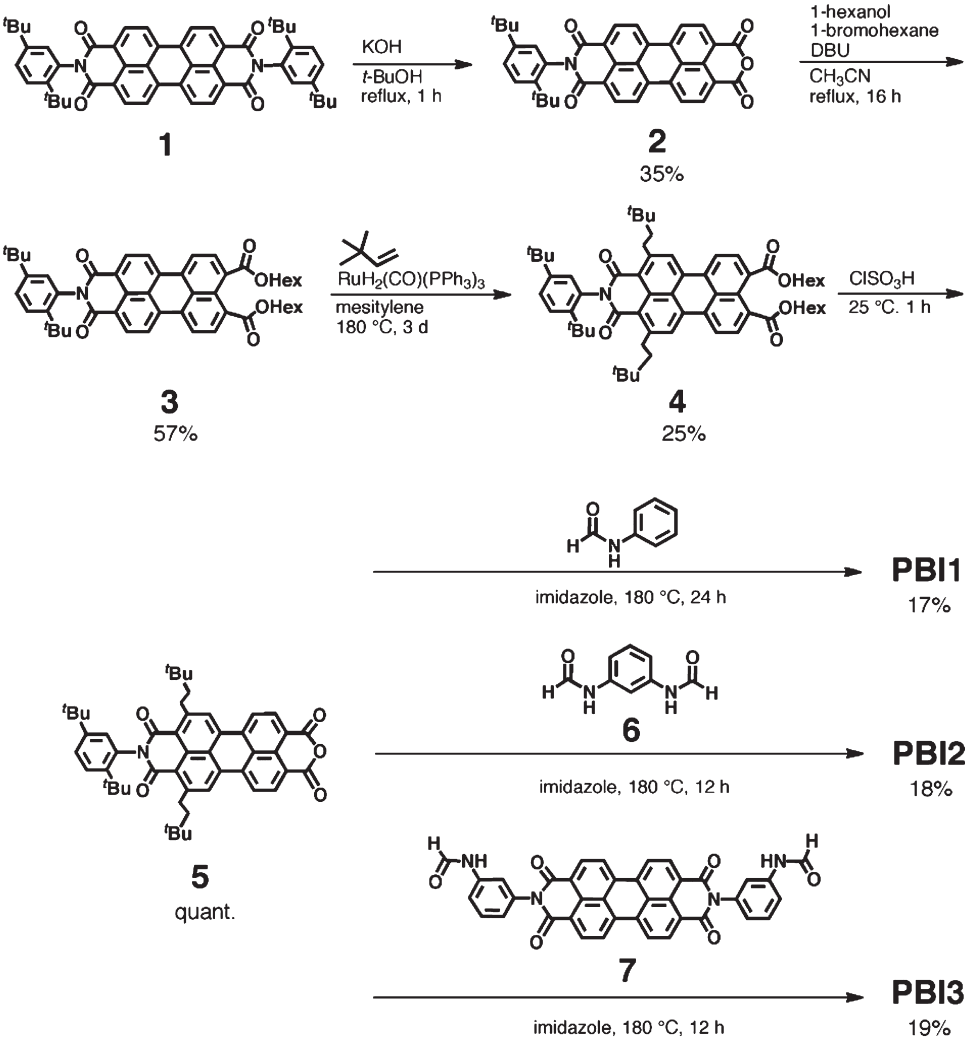

Femtosecond Transient Absorption Measurements. The femtosecond time-resolved transient absorption (TA) spectrometer consisted of homemade noncollinear optical parametric amplifier (NOPA) pumped by a Ti:sapphire regenerative amplifier system (Integra-C, Quantronix) operating at 1 kHz repetition rate and an optical detection system. The generated visible NOPA pulses had a pulse width of ~100 fs and an average power of 1 mW in the range 480−700 nm, which were used as pump pulses. White light continuum (WLC) probe pulses were generated using a sapphire window (3 mm of thickness) by focusing a small portion of the fundamental 800 nm pulses, which was picked off by a quartz plate before entering to the NOPA. The time delay between pump and probe beams was carefully controlled by making the pump beam travel along a variable optical delay (ILS250, Newport). Intensities of the spectrally dispersed WLC probe pulses are monitored by a miniature spectrograph (USB2000+, OceanOptics). To obtain the time-resolved transient absorption difference signal (ΔA) at a specific time, the pump pulses were chopped at 25 Hz, and absorption spectra intensities were saved alternately with or without pump pulse. Typically, 6000 pulses excite samples to obtain the TA spectra at a particular delay time. The polarization angle between the pump and probe beams was set at the magic angle (54.7°) using a Glan-laser polarizer with a half-wave retarder in order to prevent polarization-dependent signals. Cross-correlation fwhm in pump−probe experiments was less than 200 fs, and chirp of WLC probe pulses was measured to be 800 fs in the 400−800 nm region. To minimize chirp, all reflection optics in the probe beam path and 2 mm path length of quartz cell were used. After fluorescence and TA experiments, we carefully checked absorption spectra of all compounds to avoid artifact from degradation and photo-oxidation of samples. The HPLC grade solvents were used in all steady-state and time-resolved spectroscopic studies. The three-dimensional data sets of ΔA versus time and wavelength were subjected to singular value decomposition and global fitting to obtain the kinetic time constants and their associated spectra using Surface Xplorer software (Ultrafast Systems).

Femtosecond Transient Absorption Anisotropy Decay. A dual-beam femtosecond time-resolved transient absorption (TA) spectrometer consisted of two independently tunable homemade optical parametric amplifiers (OPA) pumped by a regeneratively amplified Ti:sapphire laser system (Hurricane-X, Spectra-Physics) operating at a 3 kHz repetition rate and an optical detection system. The OPA was based on noncollinearly phase-matching geometry, which was easily color-tuned by controlling the optical delay between white light continuum

seed pulses (450−1400 nm) and visible pump pulses (400 nm) produced by using a sapphire window and BBO crystal, respectively. The generated visible OPA pulses had a pulse width of ∼35 fs and an average power of 10 mW at 5 kHz repetition rate in the range of 500−700 nm after a fused-silica prism compressor. Two OPA pulses were used as the pump and probe pulses, respectively, for TA measurements. The probe beam was split into two parts. The one part of the probe beam was overlapped with the pump beam at the sample to monitor the transient (signal), while the other part of the probe beam was passed through the sample without overlapping the pump beam to compensate the intensity fluctuation of probe beam. The time delay between pump and probe beams was carefully controlled by making the pump beam travel along a variable optical delay (ILS250, Newport). To obtain the time-resolved transient absorption difference signal at specific wavelength, the monitoring wavelength was selected by using a narrow interface filter (fwhm ≈ 10 nm). By chopping the pump pulses at 1.5 kHz, the modulated probe pulses as well as the reference pulses were detected by two separated photodiodes (Femtowatt Photoreceiver, New Focus). The modulated signals of the probe pulses were measured by a gated integrator (SR250, SRS) and a lock-in amplifier (DSP7265, EG&G) and stored in a personal computer for further signal processing. In general experimental conditions, time resolutions of less than 50 fs were achieved. For the time-resolved transient absorption anisotropy (TAA) measurement, both $I_{\parallel}$ and $I_{\perp}$ signals were collected simultaneously by combination of polarizing beam splitter cube and dual lock-in amplifiers as the following equation:

$$r(t) = \frac{I_{\parallel} - I_{\perp}}{I_{\parallel} + 2I_{\perp}}$$

where $I_{\parallel}$ and $I_{\perp}$ represent TA singnals with the polarization of the pump and probe pulses being mutually parallel and perpendicular, respectively. The pump pulses were set to vertical polarization, and that of the probe pulse was set to 45° with respect to the pump pulse by using Glan-laser polarizers and half-wave plates. After the probe pulse passes through the sample cell, it was split by a polarizing beam splitter cube and then detected by two separated photodiodes. Two gated integrators and two lock-in amplifiers record the signal simultaneously within a single scan. As a standard, anisotropy measurement showed a clean single-exponential decay with reorientational relaxation time of 120 ps and the initial anisotropy value $r(0)$ of 0.39 for rhodamine 6G dye in methanol, which are well-matched in other reference.[19] For all TAA measurements, the wavelength of the pump and probe pulse was set to 530 and 580 nm with an average power of less than 40 μW, and a thin absorption cell with a path length of 1 mm was used to eliminate additional chirping.

Single-Molecule Spectroscopy. A confocal microscope system based on the inverted-type microscope (TE2000-U, Nikon), coupled to a picoseconds pulsed 470 nm diode laser (10 MHz repetition rate, pulse width <90 ps, LDH-F-C-470, PicoQuant), was employed for the detection of fluorescence of single molecules. The colliminated laser beam was sent to a quarter wave plate to ensure circularly polarized light and delivered to the input port of the confocal microscope after passing a beam expander to make enough beam size at the back focal plane. The laser beam was then reflected by a dichroic mirror and focused onto the sample through an oil-immersion objective lens (Plan Fluor, 1.3 NA, 100x, Nikon), passed through a dichroic mirror, cleaned with a notch filter (HNPF-470.0−1.0, Kaiser Optical Systems Inc.) and long pass filters, and focused through a 100 mm focal length lens into an active area of an avalanche photodiode (APD, SPCM-AQR-16-FC, EG&G, Perkin-Elmer). The sample positions were controlled using a piezoelectric tube scanner (XE-120, Park system). The signal from APD was delivered into a TCSPC card (SPC-830, Becker & Hickl GmbH) operated in FIFO (first-in-first-out) mode, which can construct the fluorescence intensity trajectory with a specific bin time and fluorescence decay profiles with an experimental instrument response of 500 ps. We convoluted the monoexponential fitting function with the response function to arrive at the early time rise displayed by the fits. The maximum likelihood estimation (MLE) was used to fit the fluorescence decays.[20] The detailed description of the setup and the data acquisition process has been published previously.[21]

Samples for single-molecule measurements were prepared by spin-coating solutions of the PBI oligomers (∼10^{-10} M) in dichloromethane (Aldrich, spectrophotometric grade) containing 10 mg/mL of poly(methyl methacrylate) (PMMA) (Aldrich, average M.W. 96 700) on rigorously cleaned cover glasses at 2000 rpm to yield thin polymer films (∼100 nm as measured by AFM).

RESULTS

Synthesis. Covalently linked PBI oligomers are an intriguing class of molecules for a study on single molecular fluorescence spectroscopy due to their high fluorescence quantum yields. Such oligomers, however, have been known to be notorious with respect to their low solubilities. We thus planed to introduce solubilizing groups to the PBI segment. Perylene imide-anhydride **5**, which is a key precursor for the preparation of **PBI1**, **PBI2**, and **PBI3**, was prepared following the synthetic route shown in Scheme 1.

A suspension of perylenebisimide **1** and KOH in *tert*-butanol was refluxed with vigorous stirring for 1 h, giving unsymmetric imide-anhydride **2** in 35% yield. Obtained **2** was suspended in acetonitrile, to which 1-hexanol, 1-bromohexane, and DBU were added, and the resulting mixture was refluxed for 16 h. After **2** was transformed into diester **3**, ruthenium-catalyzed C−H activating alkylation[22,23] gave imide-diester **4** in 25% yield. Treatment of **4** with chlorosulfuric acid provided **5** quantitatively. Compound **5** was condensed with formanilide and 1,3-bis(formylamino) benzene to produce **PBI1** and **PBI2** in 17 and 18% yields, respectively. Similar condensation of **5** with *N,N*-bis(3-formylaminophenyl)-substituted perylene bis-imide **7**, which was prepared from the reaction of perylene bis-anhydride with 1,3-bis(formylamino)benzene, gave **PBI3** in 19% yield. All these molecules have been fully characterized by high-resolution mass, ^{1}H NMR, and UV−vis absorption spectroscopy.

Absorption, Fluorescence Spectra, and Fluorescence Lifetimes. The normalized stationary absorption and fluorescence spectra of **PBI1**, **PBI2**, and **PBI3** in dichloromethane are presented in Figure 1 in which little bathochromic shifts were observed in the absorption and fluorescence spectra as the PBI oligomer becomes larger.

This feature indicates that the dipole coupling strengths among the PBI chromophores in **PBI2** and **PBI3** are weak. If these oligomer systems are strongly coupled, the absorption and emission spectra of PBI multichromophoric systems would be different from those of the PBI monomer. In reality, when the

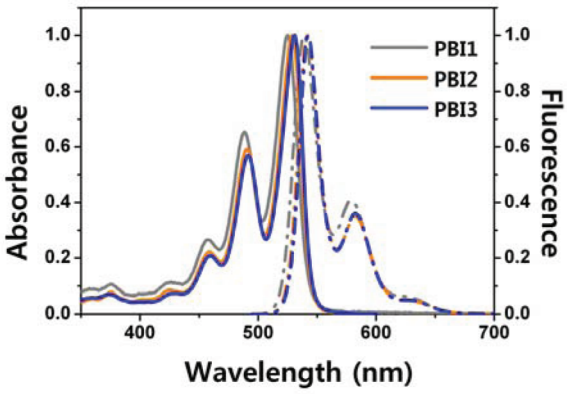

Figure 1. Normalized steady-state absorption (straight line) and fluorescence (dotted line) spectra of **PBI1**, **PBI2**, and **PBI3** in dichloromethane. The fluorescence spectra were obtained using an excitation wavelength of 470 nm.

PBI chromophores are directly linked without any linkers, a clear bathochromic shift with a few tens of nanometers and a drastic change in vibronic peak ratio were observed in the absorption and emission spectra compared with PBI monomer due to strong excitonic couplings.[15,16] Observed weak dipole coupling strengths in **PBI2** and **PBI3** can be understood by the fact that the 1,3-phenylene holds the PBI chromophores with a certain distance and nonparallel geometry. These conditions weaken the excitonic coupling strengths among the neighboring PBI units in **PBI2** and **PBI3** as compared with the directly linked PBI oligomers.

The time-resolved fluorescence decays were obtained by TCSPC technique, and their fitted fluorescence lifetimes are presented in Table 1. The fluorescence decay profiles exhibit single exponential decays with the time constants of 3.6 ns, 3.2 ns, and 3.0 ns for **PBI1**, **PBI2**, and **PBI3**, respectively, where the difference in lifetimes among **PBI1**, **PBI2**, and **PBI3** is less than 1 ns, again suggesting the weak interactions between PBI chromophores.

Table 1. Steady-State Photophysical Values and Fluorescence Lifetimes of PBI1, PBI2, and PBI3 in Dichloromethane

	λ_{abs} (max/nm)	λ_{emi} (max/nm)	Stokes shift (cm^{-1})	Φ_f[a]	τ_f (ns)[b]	k_{nr} ($\times 10^{-11} s^{-1}$)[c]
PBI1	525	539	495	0.75	3.61 ± 0.01	6.9
PB12	529	542	453	0.79	3.24 ± 0.01	6.7
PBI3	531	542	382	0.67	3.00 ± 0.01	11

[a] Φ_f indicates the fluorescence quantum yield and experimental errors are within ±0.01. [b] τ_f is the fluorescence lifetime measured by excitation at 450 nm. [c] k_{nr} is the nonradiative rate constant, which is calculated by means of following relationship: $k_{nr} = (1/\tau_f)(1 - \Phi_f)$.

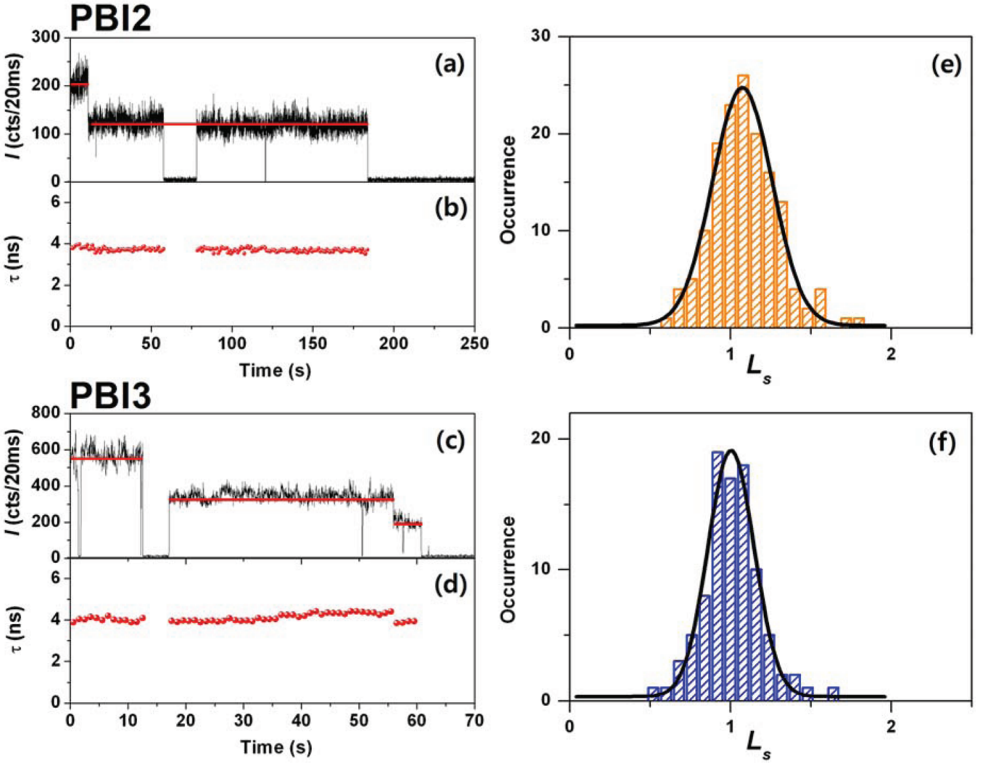

Figure 2. Single-molecule fluorescence behaviors of **PBI2** and **PBI3**. (a,c) Fluorescence intensity trajectories of **PBI2** and **PBI3**. *I* represents the number of counts per 20 ms. (b,d) Fluorescence lifetime traces, which were obtained from a group of photons for 1 s at each molecular state, and the fitted values are represented as red points. (e,f) Histograms of the superradiance coherence factor L_s (= $k_{rad,array}/k_{rad,monomer}$; $k_{rad} = \Phi_f/\tau_f$; Φ_f = fluorescence quantum yield; τ_f = fluorescence lifetime) of **PBI2** (orange) and **PBI3** (blue) in FITs. The radiative decay rates for the array and the monomer were calculated using fluorescence lifetimes at the first and last emissive levels, respectively, in the FITs and fluorescence quantum yields from bulk measurements. So, L_s values of **PBI2** and **PBI3** were calculated by using $k_{rad,dimer}/k_{rad,monomer}$ and $k_{rad,trimer}/k_{rad,monomer}$, respectively. Each histogram is fitted with a Gaussian distribution (solid line), centered at (e) 1.1 and (f) 1.0, respectively.

dx.doi.org/10.1021/jp208855u |*J. Phys. Chem. B* 2012, 116, 1244–1255

If the PBI chromophores are directly linked without any linkers, the fluorescence lifetime of the oligomer becomes much shorter than that of the monomer because of a superradiance phenomenon where the radiative coupling enhances the radiative rate of emission by forming the single quantum system.[16,24,25] Nevertheless, it is noteworthy that the fluorescence decay times of **PBI1**, **PBI2**, and **PBI3** become slightly shorter in going from **PBI1** to **PBI3**. This feature is probably due to the fact that the phenyl linker introduces a flexibility in overall molecular structures, which opens up new radiationless deactivation channels.

Single-Molecule Fluorescence Intensity and Lifetime Trajectories. Single-molecule spectroscopy (SMS) has continued to emerge as a powerful tool to study the individual behaviors of fluorescent single molecules. The SMS can provide the molecular distributions of physical quantities rather than ensemble-averaged values from bulk measurements.[26] Thus, we can obtain the spectroscopic information about the heterogeneities of energy transfer dynamics at the single molecule level.

The representative fluorescence intensity trajectories (FITs) of 253 single molecules of **PBI2** and 252 single molecules of **PBI3** spin-coated by poly(methyl methacrylate) (PMMA) are given in Figure 2a,c. Figure 2b,d represents the time traces of the fluorescence lifetimes for **PBI2** and **PBI3** fitted by every 1 s interval.

The FITs of **PBI2** and **PBI3** mainly exhibit two-step (64%) and three-step (40%) photobleaching behaviors, respectively, in accordance with the number of the constituent PBI units. These distinct levels arise from a stepwise photobleaching in a multichromophoric system. Some traces in **PBI2** show one-step photobleaching (15%), while one-step (19%) and two-step (23%) photobleachings also exist in **PBI3**. These are partly due to photobleaching of some chromophores before recording the fluorescence intensity trajectory by pre-exposure to excitation light during image scanning. The remaining traces of about 21% and 18% in the FITs of **PBI2** and **PBI3**, respectively, could not be categorized as sequential photobleaching. These traces show erratic behaviors like intensity variations more than the number of chromophores in the oligomer. These behaviors seem to originate from external factors like a proximity to the glass or air interface, quenching impurities in the polymer matrix, electron transfer between molecule and polymer, and so on.[9]

Figure 2e,f shows the histograms of the superradiance coherent factor L_s of **PBI2** (orange) and **PBI3** (blue) fitted by Gaussian distribution functions. The superradiance can be quantified using L_s, which is defined as the ratio of the radiative decay rate of the array to that of a monomer ($L_s = k_{rad,array}/k_{rad,monomer}$; $k_{rad} = \Phi_f/\tau_f$; Φ_f = fluorescence quantum yield; τ_f = fluorescence lifetime).[27] In our approach, the radiative decay rates for the array and the monomer were calculated using fluorescence lifetimes at the first and last emissive levels, respectively, in the FITs and fluorescence quantum yields from bulk measurements[28] because it is impossible to quantify them at the single-molecule level. The mean values of L_s histograms of **PBI2** and **PBI3** are 1.1 (e) and 1.0 (f), respectively, which indicates that a majority of PBI oligomers exhibit weak electronic couplings and that these features are in accordance with the results of bulk measurements. Since the coupling strength is weak, the fluorescence lifetimes in each photobleaching step are almost constant, and the magnitudes of intensities in each step do not show systematic variations (Supporting Information, S2). Slight variations in the fluorescence decays are probably due to the host matrix environment of chromophores and their conformational

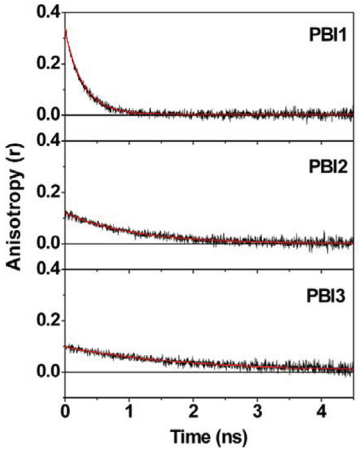

Figure 3. Time-resolved fluorescence anisotropy decay profiles of **PBI1**, **PBI2**, and **PBI3** in dichloromethane. The polarized fluorescence decays ($I_{VV}(t)$ and $I_{VH}(t)$) were measured using the excitation wavelength of 450 nm and emission wavelength of 540 nm, and then, the anisotropy decay $r(t)$ was calculated.

Table 2. Fitted Fluorescence Anisotropy Decay Parameters of PBI1, PBI2, and PBI3 in Dichloromethane[a]

	anisotropy decay parameters	
sample	r_0	τ_{rot} (ns)
PBI1	0.373 ± 0.007	0.22 ± 0.01
PBI2	0.176 ± 0.004	0.78 ± 0.03
PB13	0.120 ± 0.003	1.32 ± 0.06

[a] The fluorescence anisotropy decays were monitored at λ_{am} = 540 nm. Using the relationship $r(t) = r_0 \exp(-t/\tau_{rot})$, where $r(t)$ is the time-dependent fluorescence anisotropy $\{r(t) = [I_{\parallel}(t) - GI_{\perp}(t)]/[I_{\parallel}(t) + 2GI_{\perp}(t)]\}$, r_0 the initial anisotropy value, and τ_{rot} the fitted anisotropy decay time.

differences in the spin-coated state. However, ~7% (~3%) of **PBI2** (**PBI3**) molecules exhibit stronger electronic coupling strengths, which can delocalize the exciton state to show superradiance effects.[16] From the individual behaviors of PBI oligomers investigated by single-molecule spectroscopy, we could find some characteristic features that cannot be discovered in ensemble measurements.

Another characteristic feature in the FITs is that there are photoblinking behaviors. A well-known cause for single-molecule blinking is a transition to the triplet state.[15,29] As the decay to the ground state is symmetry-forbidden, triplet residence times typically fall in the microsecond regime, compared to nanosecond singlet excited state lifetimes. Triplet blinking is evidenced by a single-exponential distribution of microsecond-scale off times with a rate constant depending on molecular structure and nanoenvironment.[27] Apart from triplet blinking, off-times with much longer (millisecond to second) duration have also been observed in organic molecules.[30] This long-lived off state is generally ascribed to the formation of a long-lived radical−ion dark state, which originates from an electron transfer from or to trap sites (host matrix) close to the molecule.[9,31] Since the data points of fluorescence intensity were recorded by the amount of photons collected during 20 ms, the photoblinking phenomenon seems to be primarily induced by the radical−ion dark

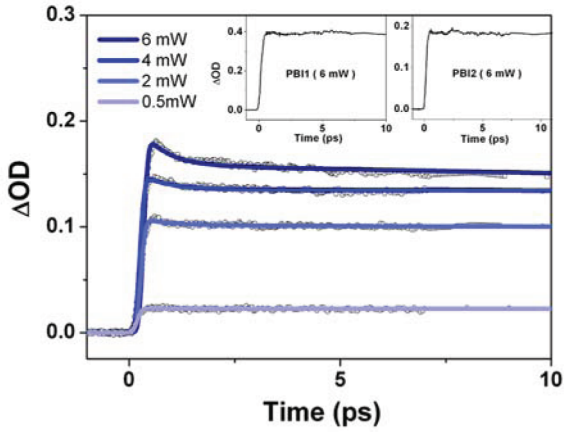

Figure 4. Transient absorption decay profile of **PBI3** that include pump-power dependence. The transient absorption decay profiles of **PBI1** and **PBI2** are shown in the insets for the comparison. In the experiments, the pump and probe wavelengths are 530 and 710 nm, which correspond to the absorption maximum excitation and induced absorption probe. The used pump beam intensities are 1.2 W/cm^2 (6 mW), 0.8 W/cm^2 (4 mW), 0.4 W/cm^2 (2 mW), and 0.1 W/cm^2 (0.5 mW).

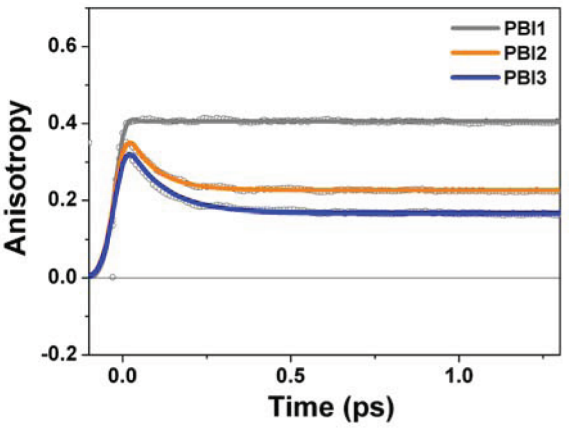

Figure 5. Transient absorption anisotropy decay profiles of **PBI1**, **PBI2**, and **PBI3** in dichloromethane. The pump and probe wavelength were 530 nm and 580 nm, respectively.

state. This photoblinking behavior is the characteristic feature of PBI molecules and their environments, regardless of whether the chromophores are strongly coupled or not.

Fluorescence Anisotropy Decay. The time-resolved fluorescence anisotropy decay profiles of **PBI1**, **PBI2**, and **PBI3** by photoexcitation at 450 nm were measured in dichloromethane (Figure 3 and Table 2).

The fluorescence anisotropy measurements to monitor the degree of depolarization are useful in these oligomer systems because the direction of the transition dipole moment in each PBI unit is different due to the overall curved structure. Thus, we can observe the causes of depolarization in these oligomers such as rotational diffusion or excitation energy transfer, which can be distinguished by a difference in the time scale between these two processes.

The fluorescence anisotropy decay times (τ_{rot}s) gradually increase from **PBI1** (0.22 ns) to **PBI2** (0.78 ns) and **PBI3** (1.32 ns) as the molecular volume of the oligomer increases. Therefore, the τ_{rot} values can be interpreted as reflecting the molecular rotational diffusion time in solution. Among the initial r_o values of **PBI1** (0.37), **PBI2** (0.17), and **PBI3** (0.12) as listed in Table 2, the r_o values of **PBI2** and **PBI3** are quite smaller than that of **PBI1**. This indicates that there is another depolarization channel in PBI multichromophores in contrast with **PBI1**. The spectral overlap between the ground-state absorption and emission spectra indicates that the fast decay channel can be considered as the intramolecular excitation energy transfer.[32,33]

On the basis of the above results, we can suggest that the coupling strength among PBI chromophore units in **PBI2** and **PBI3** is not strong enough to show the superradiance effect. Accordingly, in this case, if the intramolecular excitation energy transfer occurs, the mechanism would be the Förster-type resonance energy transfer (FRET), which proceeds after the complete relaxation of the excited donor molecule to the vibrationally equilibrium state before the energy transfer to the acceptor molecule takes place.

Table 3. Transient Absorption Decay Parameters for PBI3 in Dichloromethane[a]

	fitted decay time (ps)	
pump power (mW)	τ_1	τ_2
	PBI3	
6	0.6(20%)	3000 (80%)
4	0.6(10%)	3000 (90%)
2	0.6 (7.5%)	3000 (92.5%)
0.5	0.6	3000 (~100%)

[a] The pump and probe wavelengths are 530 and 490 nm, respectively. Using the relationship $\Delta OD(t) = A_1 \exp(-t/\tau_1) + A_2 \exp(-t/\tau_2)$, where $\Delta OD(t)$ is the transient absorption intensity, A the amplitude (noted in paretheses as the normalizes percentage, i.e., $[A_i/(A_1 + A_2)] \times 100$), and τ the fitted decay time. The experimental errors are within ~4%.

Table 4. Fitted Transient Absorption Anisotropy Decay Parameters of PBI1, PBI2, and PBI3 in Dichloromethane

	anisotropy decay parameters	
sample	r_0	τ_1 (fs)
PBI1	0.41 ± 0.02	
PBI2	0.39 ± 0.03	81 ± 8
PBI3	0.36 ± 0.02	107 ± 6

Power-Dependent Femtosecond Transient Absorption and Transient Absorption Anisotropy Decays. To investigate the fast excitation energy migration processes occurring in PBI oligomers, both pump-power dependent TA and TAA decays were measured, where the photoexcitation at 530 nm was employed to directly excite the S_1 state by eliminating the vibrational relaxation dynamics (Figures 4 and 5).

From the pump-power dependence on the TA decay, we were able to clarify the EEH process in **PBI3**. The decay profiles probed at 710 nm corresponding to the photoinduced absorption region were exponentially fitted by using two decay components (τ_1 and τ_2), where the long decay component τ_2 was

fixed as the τ value in the TCSPC measurements (Figure 4 and Table 3).

While **PBI1** and **PBI2** revealed no power dependence in the short decay component, the TA decay profile of **PBI3** was very sensitive to the pump power. As the pump power was increased, the contribution by the relatively short τ_1 (0.6 ps) component was enhanced as compared to the long τ_2 (3000 ps) one. This pump-power dependence on the TA decay is a strong indication of the singlet−singlet annihilation process.[5,6] Because the recombination between excitons that are generated simultaneously by the high density of photons makes the population of S_1 state decrease, a fast deactivation channel appears, and this probability is enhanced as the excitation power is increased.

According to the description on a natural light-harvesting system (LH1 and LH2), the singlet−singlet annihilation is conceived as a Förster-type incoherent energy hopping when the acceptor is a exciton resulting in a doubly excited acceptor state, which quickly relaxes to the singly excited state.[6,34]

While **PBI3** clearly shows the singlet−singlet annihilation process, **PBI2** does not show the enhancement of the short decay component with increasing the pump power in the TA decay profiles. Theoretically, **PBI2** can show the annihilation process, but to make this event possible, the condition that the two chromophores are excited simultaneously among two constituent units has to be satisfied, and the probability of this process is 50% lower than that of **PBI3**. Because of this harsh condition, it would be difficult to observe the short decay components in **PBI2** contributed by the singlet−singlet annihilation processes.

The depolarization process to affect the initial values of the fluorescence anisotropy can be considered as the EEH processes, but the time scale of this process seems to be too short to be observed by the fluorescence anisotropy decay through the TCSPC technique whose time-resolution is ~50 ps. Thus, the transient absorption anisotropy was employed to investigate the ultrafast depolarization process in **PBI2** and **PBI3** (Figure 5). The TAA decay profiles were probed at 580 nm corresponding to the stimulated emission region.

Figure 5 reveals the TAA decay profiles of PBI oligomers, in which fast depolarization channels appear presumably because of the EEH process. The fitted TAA decay parameters are listed in Table 4.

In contrast to **PBI1**, the decay components τ appearing before the influence of rotational motion exist in **PBI2** (0.08 ps) and **PBI3** (0.11 ps), reflecting fast depolarization processes arising from the excitation energy migration along the oligomer. This confirms the existence of intramolecular EEH processes between PBI units in a multichromophoric system.

DISCUSSION

Excitonic Coupling Strengths of PBI Oligomers. In multichromophoric assemblies, the degree of coherence determined by the excitonic coupling strength among the constituent chromophores greatly influences their photophysical properties.[16,24] When the dipole−dipole interactions are strong enough to induce radiative coupling, the coherent delocalization of the excited state is formed among the chromophores. Radiative coupling makes the electronic transition from the ground state to the lowest exciton level carry nearly all the oscillator strengths of the system, resulting in an enhancement of the radiative decay rate. Because of this cooperative excitation and emission among chromophores, the fluorescence lifetime of the strongly coupled multichromophore system becomes shorter than that of the monomer.[16] Meanwhile, after the exciton is delocalized by strong coupling over a single oligomer, the coherence length becomes shorter as the PBI units are photobleached in turn. Since the radiative coupling becomes small in parallel with the coherence length, the fluorescence lifetime of the first intensity level in the FITs would be shorter compared to the value of the last step. Also, this feature makes the fluorescence intensities decrease systematically when going to the next step in the FIT.

Scheme 2. Dipole−Dipole Interaction[a]

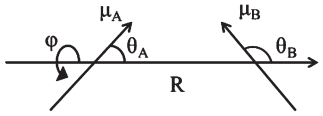

[a] The excitonic coupling strength between adjacent dipole moments (μ) is given by the angles to define the relative in-plane (θ_i) and out-of-plane (φ) orientations between the transition dipole moments A and B.

According to the point-dipole approximation,[35] the excitonic coupling strength between adjacent dipole moments is given by the angles to define the relative in-plane (θ_i) and out-of-plane (φ) orientations between the transition dipole moments A and B (Scheme 2).

$$V_{AB} = \frac{|\mu_A \mu_B|}{4\pi\varepsilon_0 R^3}(2\cos\theta_A\cos\theta_B + \sin\theta_A\sin\theta_B\cos\phi) \quad (1)$$

With the geometry optimization of **PBI2**, the center-to-center distance (R_{AB}), and angles between PBI dipoles were determined as R = 14.85 Å, θ_A = 30°, θ_B = 150°, and φ = 0°. Using the PBI dipole strength of 10 D,[36] we were able to calculate the exciton coupling strength between the PBI units. As a consequence, the coupling strength between adjacent PBI dipoles via phenylene linkage was calculated to be −96 cm^{-1}, which is similar to the experimental bathochromic shift in the absorption spectra between **PBI1** and **PBI2** (−144 cm^{-1}). It is noteworthy that the experimental value is slightly larger than the calculated one. This discrepancy is caused by the limitations of the point-dipole approximation to describe the **PBI2** whose dipole strength of each PBI unit is too large to be considered as point dipole in a given distance. The electronic coupling can also be affected by the through-bond pathways mediated by the phenylene bridge connecting donor and acceptor. These factors make the electronic coupling strength increase compared to the calculated one. However, the coupling strength is three times smaller than that of directly linked PBI dimer.[37] Also, considering the fluorescence lifetimes of **PBI2** and **PBI3** measured at the ensemble level, which do not show large differences compared to **PBI1**, we can derive that **PBI2** and **PBI3** are weakly coupled systems. The FITs measured at the single-molecule level, which exhibit similar fluorescence lifetimes among steps showing disordered intensity levels, support the weak coupling in **PBI2** and **PBI3**. Although some interactions cannot be described by typical point-dipole approximation, we can conclude that **PBI2** and **PBI3** are weakly coupled systems.

Distributions of Excitonic Coupling Strengths of PBI Oligomers at Single-Molecule Level. The distributions of superradiance coherence factor L_s of **PBI2** and **PBI3** show that

Scheme 3. Exciton Band Energy Diagram for a Dimer with Oblique Transition Dipoles[a]

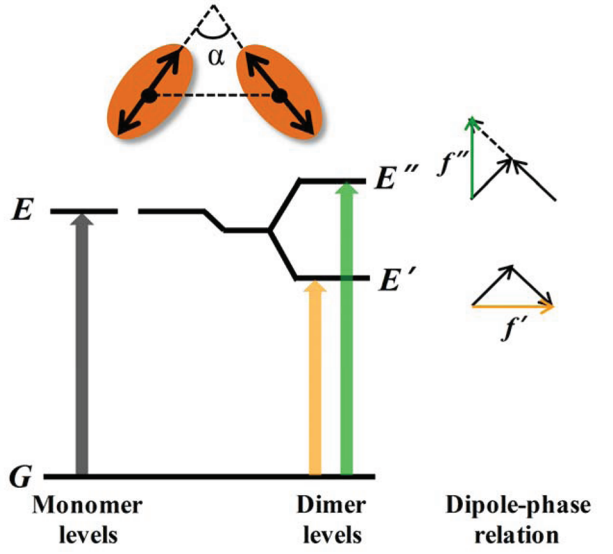

[a] The in-phase arrangement of transition dipoles (yellow) is attractive lowering the excited state energy ,and the out-of-phase arrangement of transition dipoles (green) is repulsive raising the excited state energy. α is the angle between polarization axes for the component absorbing units.

a majority of PBI oligomers exhibit weak electronic couplings. However, some of PBI oligomers (~7% of **PBI2** and ~3% of **PBI3**) show stronger electronic couplings. In a dimer system, if the excitation is completely delocalized, the superradiance coherence factor L_s becomes 2 ($L_s = k_{rad,dimer}/k_{rad,monomer}$).[37] However, at room temperature in a polymer matrix, both static (dye energy fluctuation introduced by polymer host) and dynamic (exaction−phonon coupling) disorders may limit the exciton delocalization and result in a decrease of L_s values. In reality, biperyleneimide, where dye units are connected directly, shows L_s values ranging from 1 to 1.8.[37] In this regard, the molecules whose L_s values are over 1.5 are considered as strongly coupled ones, which could partially delocalize the exciton.[37] According to this result, about 7% of **PBI2** exhibit strong electronic couplings. From the previous study on the exciton coherence of the directly linked PBI trimer, we can derive that ~3% of **PBI3** exhibit a partially delocalized excitonic state (L_s = ~1.5).[16] It is noteworthy that **PBI2** molecules show stronger electronic couplings than **PBI3**, which can be explained by Kasha's exciton band energy diagram of oblique dimer.[25]

Oblique transition dipoles of the dimer system lead to the exciton energy diagram are shown in Scheme 3. In this case, the in-phase arrangement of transition dipoles for the monomer is attractive and leads to a lowering of energy (E'), and the out-of-phase arrangement of transition dipoles is repulsive and causes a raising of the excited state energy (E'') in the dimer system. qThe transition dipole moment f', which is formed by the in-phase arrangement of transition dipoles, is related to the delocalized exciton. Since the transition dipole moment strength f' of **PBI2** increases along with the angle α between two transition dipoles, the molecular structure can influence the oscillator strength of delocalized excitonic state E'. When the molecules are spin-coated with the polymer, they are confined in a free volume of polymer host that could compress or deform the molecular structure in contrast with the solution phase. Because **PBI3** is bulkier than **PBI2**, **PBI3** would be more compressed, and this feature decreases the angle α, which weakens the transition dipole moment f' strength. Considering this mechanism, **PBI2** is more likely to reach the delocalized excitonic state than **PBI3**, which explains that the L_s values over 1.5 appear more often in **PBI2**. Also, the effects of static and dynamic disorders would be lager in **PBI3**, which is bulker than **PBI2**, and this could decrease the portion of strongly coupled conformations in **PBI3** than **PBI2**.

Incoherent Förster-Type Energy Transfer in PBI Oligomers. We have estimated the excitation energy transfer processes within **PBI2** and **PBI3** using the anisotropy depolarization and singlet−singlet annihilation processes, respectively, and compared the results with the FRET model to identify the EEH processes.

The experimentally deduced EEH time in **PBI2** can be obtained from the short decay component of the TAA decay profile. Because **PBI2** is a dimer, we can think that the EEH process of **PBI2** is reversible between PBI units like a simple equilibrium scheme as follows,

$$PBI_A^* PBI_B \rightleftarrows PBI_A PBI_B^*$$

where PBI and PBI* represent ground and excited state PBI units, and k_1 and k_{-1} are forward and backward reaction rate constants, respectively. Thus, the EEH rate constant for the above reaction scheme can be defined by eq 2.

$$\tau_d = \frac{1}{k_1 + k_{-1}} \quad (2)$$

where τ_d is the measured anisotropy decay time of **PBI2**. Since **PBI2** consists of identical monomer PBI units, the rate constants k_1 and k_{-1} are the same. Using eq 2, the EEH rate constant via the phenyl linker of **PBI2** was determined to be 6.2×10^{12} s^{-1}, and the EEH time is τ_h = 0.16 ps.

From the decay of the TA power dependence signal reflecting the singlet−singlet annihilation process, we can derive the excitation energy hopping time of **PBI3**. However, since the annihilation time does not represent the energy hopping time straightforwardly, a modeling of energy migration is necessary.

In a molecular ring structure such as the bacterial light-harvesting complex of LH1, a kinetic analysis of singlet−singlet annihilation is well-known as eq 3 by assuming the annihilation process as a random walk of one excitation with respect to another fixed excitation[38,39]

$$\tau_a^{ring} = \frac{\tau_h}{8 \sin^2(\pi/2N)} \quad (3)$$

where τ_a^{ring} is the annihilation lifetime in the ring structure, τ_h is the exciton hopping time, and N is the number of hopping sites in the ring. By using the simple symmetry arguments, we can extend the annihilation kinetics to open chain, and as a result, the annihilation lifetime for the open chain is just twice long as that of the closed one.[38]

$$\tau_a^{chain} = 2\tau_a^{ring} \quad (4)$$

In **PBI3**, τ_a^{chain} is 0.60 ps, and the number of hopping sites N is 3, so the hopping time of **PBI3** is 0.60 ps. Finally, the calculated

EEH rate constant based on the Förster theory can be obtained from the following eqs 5 and 6:[40]

$$R_0 = \left(\frac{9000(\ln 10)\kappa^2\Phi_D J}{128\pi^5 n^4 N_A}\right)^{1/6} \quad (5)$$

$$k_{ET} = \frac{1}{\tau_D}\left(\frac{R_0}{R}\right)^6 \quad (6)$$

where R_0 is the critical distance, κ^2 the orientation factor that describes the relative orientation of the donor and acceptor transition dipoles, Φ_D the fluorescence quantum yield of donor in the absence of acceptor, J the extent of spectral overlap between donor emission and acceptor absorption spectrum, n the refractive index of medium, and N_A the Avogadro's constant in eq 5. In eq 6, k_{ET} is the rate constant of the Förster-type energy transfer, τ_D the fluorescence lifetime of donor in the absence of acceptor, and R the distance between PBI units. When applying the above Förster theory to the **PBI2** system, only the dipole−dipole Coulombic interaction between donor and acceptor was considered (point-dipole approximation).

The center-to-center distance between PBI units is 14.85 Å based on the optimized structure. The orientation factor, κ^2 is 1.56 (Supporting Information, S3), and the spectral overlap, J, was measured as 7.84×10^{14} M^{-1} cm^{-1} nm^4 experimentally, whose error range is within ~4%. Using the previous parameters, the Förster radius, R_0 which is the distance where the energy transfer rate is equal to the fluorescence decay rate, was calculated as 51.90 ± 0.02 Å. This corresponds to the typical values ranging from 10 to 80 Å for the Förster distance reported in the literature.[41] According to this value, the EEH rate constant of **PBI2** was determined to be 5.08×10^{11} s^{-1}, leading to the EEH time of τ_h = 1.97 ps. Considering the EEH times of **PBI2** (0.16 ps) and **PBI3** (0.60 ps) derived from the two different spectroscopic observables, anisotropy depolarization and singlet−singlet annihilation, along with the Förster-type EEH time (1.97 ps), the excitation energy transfer mechanism of PBI oligomers could be described by the Förster-type incoherent energy hopping model. However, the EEH times obtained from the time-resolved spectroscopic experiments are somewhat shorter than the Förster-type EEH times. The discrepancies in excitation energy transfer times compared with the experimental values could be explained by the previous studies.[42] The deviations from the $1/R^6$ distance dependence of the FRET rate are caused by short interchromophoric separations because the point-dipole approximation has a limitation to describe **PBI2**. The short distance between PBI units makes it difficult to treat the PBI moiety as a point dipole. According to the recent work on FRET, when the dipole approximation becomes inadequate because of a close proximity between chromophores, higher order terms of the multipole expansion are necessary to obtain a correct description of the Coulombic coupling.[42a] Several mathematical approaches have been developed for this purpose such as the transition density cube method.[43] By using such methods, the discrepancy would be overcome to some extent. The second reason is the Dexter-type energy transfer.[44] This energy transfer mechanism is also called as short-range or exchange energy transfer, which occurs as a result of the electron exchange mechanism, mediated by an orbital overlap between energy donor and acceptor. In the cases of **PBI2** and **PBI3**, the through-bond electronic coupling can be operative because the donor/acceptor orbitals can be mixed slightly by the short phenylene linker. This effect is attributable to the deviations from the Förster theory. Evidence on the electronic coupling beyond the through-space interactions can be found in the absorption spectra. Since the through-space interaction between donor and acceptor is weak, no perturbations should be observed in the intrinsic spectroscopic properties of participants.[33] However, the steady-state spectra show small bathochromic shifts when the oligomers become longer displaying the slightly decreased vibronic ratios of **PBI2** and **PBI3** compared with those of **PBI1**. These through-bond effects contribute to the EEH times obtained from the spectroscopic measurements which are shorter than the Förster-type ones.

CONCLUSIONS

We have synthesized the 1,3-phenylene linked PBI oligomers and investigated the excitation energy transfer processes. At room temperature, the ensemble and single-molecule measurements indicate that the constituent PBI units are weakly coupled in these PBI oligomers. Similar fluorescence lifetimes at the ensemble level between **PBI1** and **PBI3** and no lifetime differences between different fluorescence intensity levels in the FITs at the single molecule level support this feature, although few PBI oligomers investigated by single-molecule spectroscopy exhibit stronger intramolecular electronic couplings than ensemble-averaged values. In the weakly coupling case, the excitation energy transfer occurs through the Förster-type incoherent energy transfer mechanism. Actually, the EEH time via the phenyl linker in **PBI2** probed by the anisotropy depolarization is 0.16 ps, and that of **PBI3** revealed by the singlet−singlet annihilation process is 0.60 ps, which is close to the EEH time of 1.97 ps derived from the Förster theory. The observed short EEH times compared to similar PBI oligomer structures are attributed to the limitation of the point-dipole approximation to describe the PBI oligomers because of the short interchromophoric distance. Also, the orbital overlap between donor and acceptor causes the deviations from the Förster theory.[44] Summarizing the photophysical properties of 1,3-phenylene-linked PBI oligomer systems, we could suggest that these energy transport characters help PBI oligomers to be good candidates as molecular photonic devices such as an artificial light-harvesting system.

ASSOCIATED CONTENT

Supporting Information. Details of synthetic procedures, ^{1}H NMR, time-resolved fluorescence decay profiles, additional single-molecule fluorescence intensity trajectories, and procedure of calculating orientation factor. This material is available free of charge via the Internet at http://pubs.acs.org.

AUTHOR INFORMATION

Corresponding Author

*E-mail: dongho@yonsei.ac.kr (D.K.); osuka@kuchem.kyoto-u.ac.jp (A.O.).

ACKNOWLEDGMENT

The work at Yonsei University was supported by the Mid-career Researcher Program (2010-0029668) and World Class University (*R*32-2010-000-10217) Programs of the Ministry of Education, Science, and Technology (MEST) of Korea. The

work at Kyoto University was supported by Grant-in-Aids for Scientific Research (20550047 (A) and 21108517 (π-space)) from the Japanese Ministry of Education, Culture, Sports, Science and Technology. The quantum calculations were performed using the supercomputing resources of the Korea Institute of Science and Technology Information (KISTI).

REFERENCES

(1) (a) Huber, R. *Angew. Chem., Int. Ed.* **1989**, *28*, 848–869. (b) Holzwarth, A. R. In *Series on Photoconversion of Solar Energy*; Archer, M. D., Barber, J., Eds.; Imperial College Press: London, U.K., 2002; pp 43−115. (c) Pullerits, T.; Sundström, V. *Acc. Chem. Res.* **1996**, *29*, 381–389. (d) Cogdell, R. J.; Lindsay, J. G. *New Phytol.* **2000**, *145*, 167–196. (e) Hu, X.; Ritz, T.; Damjanović, A.; Autenrieth, F.; Schulten, K. *Q. Rev. Biophys.* **2002**, *35*, 1–62.

(2) (a) Scandola, F.; Indelli, M. T.; Chiorboli, C.; Bignozzi, C. A. *Top. Curr. Chem.* **1990**, *158*, 73–149. (b) Wasielewski, M. R. *Chem. Rev.* **1992**, *92*, 435–461. (c) Hoeben, F. J. M.; Jonkheijm, P.; Meijer, E. W.; Schenning, A. P. H. J. *Chem. Rev.* **2005**, *105*, 1491–1546. (d) Gust, D.; Moore, T. A.; Moore, A. L. *Acc. Chem. Res.* **2001**, *34*, 40–48. (e) Wasielewski, M. R. *J. Org. Chem.* **2006**, *71*, 5051–5066.

(3) *Supramolecular Dye Chemistry*, Topics in Current Chemistry; Würthner, F., Ed.; Springer-Verlag: Berlin, Germany, 2005; Vol. 258.

(4) (a) Nakamura, Y.; Hwang, I.-W.; Aratani, N.; Ahn, T. K.; Ko, D. M.; Takagi, A.; Kawai, T.; Matsumoto, T.; Kim, D.; Osuka, A. *J. Am. Chem. Soc.* **2005**, *127*, 236–246. (b) Hwang, I.-W.; Park, M.; Ahn, T. K.; Yoon, Z. S.; Ko, D. M.; Kim, D.; Ito., F.; Ishibashi, Y.; Khan, S. R.; Nagasawa, Y.; Miyasaka, H.; Ikeda, C.; Takahashi, R.; Ogawa, K.; Satake, A.; Kobuke, Y. *Chem.—Eur. J.* **2005**, *11*, 3753–3761. (c) Cho, H. S.; Rhee, H.; Song, J. K.; Min, C.-K.; Takase, M.; Aratani, N.; Cho, S.; Osuka, A.; Joo, T.; Kim, D. *J. Am. Chem. Soc.* **2003**, *125*, 5849–5860.

(5) Hwang, I.-W.; Kamada, T.; Ahn, T. K.; Ko, D. M.; Nakamura, T.; Tsuda, A.; Osuka, A.; Kim, D. *J. Am. Chem. Soc.* **2004**, *126*, 16187.

(6) Hwang, I.-W.; Ko, D. M.; Ahn, T. K.; Yoon, Z. S.; Peng, X.; Aratani, N.; Kim, D.; Osuka, A. *J. Phys. Chem. B* **2005**, *109*, 8643–8651.

(7) (a) Schlichting, P.; Duchscherer, B.; Seisenberger, G.; Basché, T.; Bräuchle, C.; Müllen, K. *Chem.—Eur. J.* **1999**, *5*, 2388–2395. (b) Prathapan, S.; Yang, S. I.; Seth, J.; Miller, M. A.; Bocian, D. F.; Holten, D.; Lindsey, J. S. *J. Phys. Chem. B* **2001**, *105*, 8237–8248. (c) Loewe, R. S.; Tomizaki, K.-Y.; Youngblood, W. J.; Bo, Z.; Lindsey, J. S. *J. Mater. Chem.* **2002**, *12*, 3438–3451. (d) Ego, C.; Marsitzky, D.; Becker, S.; Zhang, J.; Grimsdale, A. C.; Müllen, K.; MacKenzie, J. D.; Silva, C.; Friend, R. H. *J. Am. Chem. Soc.* **2003**, *125*, 437–443. (e) Hinze, G.; Haase, M.; Nolde, F.; Müllen, K.; Basché, T. *J. Phys. Chem. A* **2005**, *109*, 6725–6729.

(8) (a) Moore, A. L. *Acc. Chem. Res.* **1993**, *26*, 198. (b) Gust, D.; Moore, T. A.; Moore, A. L. *Acc. Chem. Res.* **2001**, *34*, 40. (c) Holton, D.; Bocian, D. F.; Linsey, J. S. *Acc. Chem. Res.* **2002**, *35*, 57.

(9) Vosch, T.; Fron, E.; Hotta, J. I.; Deres, A.; Uji-i, H.; Idrissi, A.; Yang, J.; Kim, D.; Puhl, L.; Haeuseler, A.; Müllen, K.; De Schryver, F. C.; Sliwa, M.; Hofkens, J. *J. Phys. Chem. C* **2009**, *113*, 11773–11782.

(10) Hippius, C.; Van Stokkum, I. H. M.; Gsä1nger, M.; Groeneveld, M. M.; Williams, R. M.; Wü1rthner, F. *J. Phys. Chem. C* **2008**, *112*, 2476–2486.

(11) (a) Chiu, T. L.; Xu, W. F.; Lin, C. F.; Lee, J. H.; Chao, C. C.; Leung, M. K. *Appl. Phys. Lett.* **2009**, 94. (b) Metivier, R.; Nolde, F.; Müllen, K.; Basche, T. *Phys. Rev. Lett.* **2007**, *98*, 047802/1–047802/4. (c) Jung, C.; Müller, B. K.; Lamb, D. C.; Nolde, F.; Müllen, K.; Bräuchle, C. *J. Am. Chem. Soc.* **2006**, *15*, 5283–5291. (d) Kirstein, J.; Platschek, B.; Jung, C.; Brown, R.; Bein, T.; Bräuchle, C. *Nat. Mater.* **2007**, *6*, 303–310. (e) Holman, M. W.; Liu, R. C.; Adams, D. M. *J. Am. Chem. Soc.* **2003**, *125*, 12649–12654. (f) Gomez, R.; Veldman, D.; Blanco, R.; Seoane, C.; Segura, J. L.; Janssen, R. A. J. *Macromolecules* **2007**, *40*, 2760–2772. (g) Melnikov, S. M.; Yeow, E. K. L.; Uji-I, H.; Cotlet, M.; Müllen, K.; De Schryver, F. C.; Enderlein, J.; Hofkens, J. *J. Phys. Chem. B* **2007**, *111*, 708–719.

(12) (a) Serin, J. M.; Brousmiche, D. W.; Fréchet, J. M. J. *J. Am. Chem. Soc.* **2002**, *124*, 11848–11849. (b) Gronheid, R.; Stefan, A.; Cotlet, M.; Hofkens, J.; Qu, J.; Müllen, K.; Van der Auweraer, M.; Verhoeven, J. W.; De Schryver, F. C. *Angew. Chem., Int. Ed.* **2003**, *42*, 4209–4214. (c) De Schryver, F. C.; Vosch, T.; Cotlet, M.; Van der Auweraer, M.; Müllen, K.; Hofkens, J. *Acc. Chem. Res.* **2005**, *38*, 514–522. (d) Serin, J. M.; Brousmiche, D. W.; Fréchet, J. M. J. *Chem. Commun.* **2002**, 2605–2607. (e) Gronheid, R.; Hofkens, J.; Köhn, F.; Weil, T.; Reuther, E.; Müllen, K.; De Schryver, F. C. *J. Am. Chem. Soc.* **2002**, *124*, 2418–2419. (f) Weil, T.; Reuther, E.; Müllen, K. *Angew. Chem., Int. Ed.* **2002**, *41*, 1900–1904. (g) Jordens, S.; De Belder, G.; Lor, M.; Schweitzer, G.; Van der Auweraer, M.; Weil, T.; Reuther, E.; Müllen, K.; De Schryver, F. C. *Photochem. Photobiol. Sci.* **2003**, *2*, 177–186.

(13) (a) Chiu, T. L.; Chuang, K. H.; Lin, C. F.; Ho, Y. H.; Lee, J. H.; Chao, C. C.; Leung, M. K.; Wan, D. H.; Li, C. Y.; Chen, H. L. *Thin Solid Films* **2009**, *517*, 3712–3716. (b) Cölle, M.; Tsutsui, T. *Synth. Met.* **2000**, *111*−*112*, 95–97.

(14) Sliwa, M.; Flors, C.; Oesterling, I.; Hotta, J.; Müllen, K.; De Schryver, F. C.; Hofkens, J. *J. Phys.: Condens. Matter* **2007**, 19.

(15) Hoogenboom, J. P.; Hernando, J.; van Dijk, E.; van Hulst, N. F.; Garcia-Parajo, M. F. *ChemPhysChem.* **2007**, *8*, 823–833.

(16) Hernando, J.; Hoogenboom, J. P.; van Dijk, E. M. H. P.; Garcia-Lopez, J. J.; Crego-Calama, M.; Reinhoudt, D. N.; van Hulst, N. F.; Garcia-Parajo, M. F. *Phys. Rev. Lett.* **2004**, *93*, 236404.

(17) (a) Han, J. J.; Shaller, A. D.; Wang, W.; Li, A. D. Q. *J. Am. Chem. Soc.* **2008**, *130*, 6974–6982. (b) Yoo, H.; Yang, J.; Yousef, A.; Wasielewski, M. R.; Kim, D. *J. Am. Chem. Soc.* **2010**, *132*, 3939–3944. (c) Hippius, C.; Van Stokkum, I. H. M.; Zangrando, E.; Williams, R. M.; Wykes, M.; Beljonne, D.; Würthner., F. *J. Phys. Chem. C* **2008**, *112*, 14626–14638.

(18) (a) Hajjaj, F.; Yoon, Z. S.; Yoon, M. C.; Park, J.; Satake, A.; Kim, D.; Kobuke, Y. *J. Am. Chem. Soc.* **2006**, *128*, 4612–4623. (b) Nakamura, Y.; Hwang, I.-W.; Aratani, N.; Ahn, T. K.; Ko, D. M.; Takagi, A.; Kawai, T.; Matsumoto, T.; Kim, D.; Osuka, A. *J. Am. Chem. Soc.* **2005**, *127*, 236–246.

(19) Philips, L. A.; Webb, S. P.; Yeh, S. W.; Clark, J. H. *J. Phys. Chem.* **1985**, *89*, 17.

(20) Maus, M.; Cotlet, M.; Hofkens, J.; Gensch, T.; De Schryver, F. C.; Schaffer, J.; Seidel, C. A. M. *Anal. Chem.* **2001**, *73*, 2078.

(21) Vosch, T.; Cotlet, M.; Hofkens, J.; Van Der Biest, K.; Lor, M.; Weston, K.; Tinnefeld, P.; Sauer, M.; Latterini, L.; Müllen, K.; De Schryver, F. C. *J. Phys. Chem. A* **2003**, *107*, 6920.

(22) Nakazono, S.; Imazaki, Y.; Yoo, H.; Yang, J.; Sasamori, T.; Tokitoho, N.; Cédric, T.; Kageyama, H.; Kim, D.; Shinokubo, H.; Osuka, A. *Chem.—Eur. J.* **2009**, *15*, 7530–7533.

(23) Nakazono, S.; Easwaramoorthi, S.; Kim, D.; Shinokubo, H.; Osuka, A. *Org. Lett.* **2009**, *11*, 5426–5429.

(24) (a) Davydov, A. S. *Theory of Molecular Excitons*; Plenum: New York, 1971. (b) Kasha, M.; Rawls, H. R.; El-Bayoumi, M. A. *Pure Appl. Chem.* **1965**, *11*, 371.

(25) Kasha, M.; Rawls, H. R.; El-Bayoumi, M. A. *Pure Appl. Chem.* **1965**, *11*, 371.

(26) (a) Lu, H. P.; Xie, X. S. *J. Phys. Chem. B* **1997**, *101*, 2753. (b) Ha, T.; Enderle, T.; Chemla, D. S.; Selvin, P. R.; Weiss, S. *Phys. Rev. Lett.* **1996**, *77*, 3979.

(27) (a) Pullerits., T.; Chachisvilis., M.; Sundström., V. *J. Phys. Chem.* **1996**, *100*, 10787–10792. (b) Zhao, Y.; Meier., T.; Zhang., W. M.; Chernyak., V.; Mukamel, S. *J. Phys. Chem. B* **1999**, *103*, 3954–3962.

(28) Yang, J.; Yoo, H.; Aratani, N.; Osuka, A.; Kim, D. *Angew. Chem., Int. Ed.* **2009**, *48*, 4323–4327.

(29) (a) Veerman, J. A.; Garcia-Parajo, M. F.; Kuipers, L.; Van Hulst, N. F. *Phys. Rev. Lett.* **1999**, *83*, 2155. (b) Tinnefeld, P.; Hofkens, J.; Herten, D. P.; Masuo, S.; Vosch, T.; Cotlet, M.; Habuchi, S.; Müllen, K.; De Schryver, F. C.; Sauer, M. *ChemPhysChem* **2004**, *5*, 1786. (c) Haase, M.; HSbner, C. G.; Reuther, E.; Herrmann, A.; Müllen, K.; Basche, T. *J. Phys. Chem. B* **2004**, *108*, 10445.

(30) (a) Liu, R.; Holman, M. W.; Zang, L.; Adams, D. M. *J. Phys. Chem. A* **2003**, *107*, 6522. (b) Schuster, J.; Cichos, F.; Von Borczyskowski, C. *Appl. Phys. Lett.* **2005**, *87*, 051915.

(31) Zondervan, R.; Kulzer, F.; Orlinskii, S. B.; Orrit, M. *J. Phys. Chem. A* **2003**, *107*, 6770.

(32) Wu, P.; Brand, L. *Anal. Biochem.* **1994**, *218*, 1–13.

(33) Förster, T. *Discuss. Faraday Soc.* **1959**, 7–17.
(34) (a) Bradforth, S. E.; Jimenez, R.; Van Mourik, F.; Van Grondelle, R.; Fleming, G. R. *J. Phys. Chem.* **1995**, *99*, 16179. (b) Trinkunas, G.; Herek, J. L.; Polívka, T.; Sundström, V.; Pullerits, T. *Phys. Rev. Lett.* **2001**, *86*, 4167. (c) Trinkunas, G. *J. Lumin.* **2003**, *102*, 532. (d) Brüggemann, B.; May, V. *J. Chem. Phys.* **2004**, *120*, 2325. (e) Müller, M. G.; Hucke, M.; Reus, M.; Holzwarth, A. R. *J. Phys. Chem.* **1996**, *100*, 9537. (f) Brüggemann, B.; Herek, J. L.; Sundström, V.; Pullerits, T.; May, V. *J. Phys. Chem. B* **2001**, *105*, 11391.
(35) (a) Kasha, M. *Radiat. Res.* **1963**, *20*, 55. (b) Scholes, G. D.; Ghiggino, K. P. *J. Phys. Chem.* **1994**, *98*, 4580.
(36) Ernst, D.; Hildner, R.; Hippius, C.; Würthner, F.; Köhler, J. *Chem. Phys. Lett.* **2009**, *482*, 93–98.
(37) Lippitz, M.; Hübner, C. G.; Christ, T.; Eichner, H.; Bordat, P.; Herrmann, A.; Müllen, K.; Bashché, T. *Phys. Rev. Lett.* **2004**, *92*, 103001.
(38) Trinkunas, G. *J. Lumin.* **2003**, *102*−*103*, 532–535.
(39) Trinkunas, G. *Phys. Rev. Lett.* **2001**, *86*, 4167.
(40) Lakowicz, J. R. *Principles of Fluorescence Spectroscopy*; Springer: New York, 2006.
(41) Valeur, B. *Molecular Fluorescence*; Wiley-VCH: Weinheim, Germany, 2002; pp 247−272.
(42) (a) Beljonne, D.; Curutchet, C.; Scholes, G. D.; Silbey, R. J. *J. Chem. Phys. B* **2009**, *113*, 6583–6599. (b) Langhals, H.; Esterbauer, A. J.; Walter, A.; Riedle, E.; Pugliesi, I. *J. Am. Chem. Soc.* **2010**, *132*, 16777–16782. (c) Curutchet, C.; Feist, F. A.; Van Averbeke, B.; Mennucci, B.; Jacob, J.; Müllen, K.; Basché, T.; Beljonne, D. *Phys. Chem. Chem. Phys.* **2010**, *12*, 7378–7385.
(43) Regner, T. *Photosynth. Res.* **2009**, *102*, 471–485.
(44) (a) Dexter, D. *J. Chem. Phys.* **1953**, *21*, 836–850. (b) Dexter, D. L.; Schulman, J. H. *J. Chem. Phys.* **1954**, *22*, 1063–1070.